Unsteady Aerodynamic Considerations in the Design of a Drag-Reduction Spike

J. Peter Reding,* Rolf A. Guenther,† and Bernard J. Richter‡
Lockheed Missiles & Space Company, Inc., Sunnyvale, Calif.

The Trident I Missile features an extendible nose spike that reduces the drag of the blunt nose by creating a low dynamic-pressure flow separation. Experience with the Apollo-Saturn boosters indicates that the flow separation could contribute negative aerodynamic damping to certain critical free-free bending modes. It is essential to determine if the undamping is severe enough to endanger the missile structural integrity. The aerodynamic damping analysis is presented, including the effects of discontinuous spike deflection that occurs when thermal expansion, due to aerodynamic heating, loosens the spike joints. Fluctuating-pressure wind-tunnel test data are also included since the fluctuating pressures produce the most severe lateral aerodynamic load on the "aerospike".

Nomenclature

A = axial force; coefficient $C_A = A/(\rho U^2 S)/2$
B = $\rho U^2 S/2\hat{m}$
c = reference length (missile maximum diameter)
D = damping derivative
D_a, D_s = aerodynamic damping derivative attached and separated flow, respectively
$\bar{D}$ = average aerodynamic damping derivative over one cycle
f = frequency
$\bar{K}, \bar{K}_a$ = structural and aerodynamic spring constant averaged over one cycle, respectively
m = pitching moment; coefficient, $C_m = m/(\rho U^2 Sc)/2$
$\hat{m}$ = generalized mass
S = reference area; $S = \pi c^2/4$
t = time
P = pressure
q = normalized coordinate, dynamic pressure
rms = root-mean square
U = flow velocity
x, z = axial and vertical coordinate, respectively
α = angle of attack
β = spike displacement angle
Δ = increment
γ = $\omega\Delta t$
ρ = air density
ω = circular frequency
$\bar{\omega}$ = $\omega c/U$
ζ_a, ζ = aerodynamic and structural damping fraction of critical, respectively
ξ = x/c
θ = pitch attitude
ϕ = normalized modal deflection
ψ = phase angle, ωt
∞ = freestream flow

Subscripts

a = attached flow
c = critical
D = discontinuity
J = jump
s = separated flow or spike
T = spike tip
$T.E.$ = trailing edge
u = upstream
0 = denotes trim condition
$1, 2,$ etc. = numbering subscripts

Superscripts

i = induced, e.g., $\Delta^i C_N$ = induced normal force
$'$ = derivative with respect to x (d/dx)
$\cdot$ = derivatime with respect to time (d/dt)
$\cdot\cdot$ = double derivative with respect to time (d^2/dt^2)

Presented at the AIAA/ASME/SAE 17th Structures, Structural Dynamics, and Materials Conference, King of Pressia, Pa. May 5-7, 1976 (in bound volume of Conference Papers, no preprint number); submitted June 28, 1976; revision received Oct. 29, 1976.

Index categories: Aeroelasticity and Hydroelasticity; Nonsteady Aerodynamics; Jets, Wakes, and Viscid-Inviscid Flow Interactions.

*Research Specialist. Member, AIAA.
†Senior Aerodynamics Engineer.
‡Staff Engineer.

Introduction

As larger missiles are housed within launch tubes designed for smaller predecessors, the missile nose becomes more blunt to make more efficient use of the available launch tube volume. This results in a significant performance penalty due to increased nose drag. In order to minimize the nose drag, the missile has been supplied with an extendible nose spike. The spike creates a region of flow separation over the nose (Fig. 1) that reduces the drag (Fig. 2)[1] due to the reduced dynamic pressure in the separated region.[2]

Experience with the Apollo-Saturn boosters, where the escape rocket produces a flowfield similar to that of the drag reduction spike, indicates that the spike-induced separation can cause aerodynamic undamping of certain critical modes. It was the damping of the tail fins that saved the Apollo-Saturn I from aeroelastic instability,[3] but the Trident I does not have tail fins. Modal undamping then appears possible.

Spike-Body Aerodynamics

The undamping is the result of an increase in the nose-normal force derivative that results when the low dynamic-pressure flow separation is swept to the leeward side of the nose at angle of attack. This effect was measured in the wind tunnel by testing models with deflected spikes and carpet-plotting the results[4] similar to earlier investigations of wake generators.[5,6] The spike also reduces the effect of local crossflow on the nose due to the reduced dynamic pressure in the separated region. Thus, two normal force components exist in the separated region on the nose (Fig. 2). One due to the translation of the spike

$$C_N = (\partial C_N/\partial z)z = (\partial C_N/\partial\beta)\beta \qquad (1)$$

where $\beta=(z/c)(\xi_T-\xi_s)$ for small z, and another due to local cross flow

$$C_{Ns}=(\partial C_N/\partial\alpha_s)\alpha_s=C_{N\alpha}(q_s/q)\alpha_s \tag{2}$$

where s denotes separated flow load.

Furthermore, the dynamic pressure ratio in the separated region has been related to the axial force ratio[3] $q_s/q=C_{Aos}/C_{A0}$ which has been verified experimentally.[7,8]

Quasisteady Analysis

One can easily see that as the vehicle oscillates (or pitches), the induced load will not occur instantaneously due to the position of the spike tip, but will lag due to the finite convection speed in the separated region. That is, the quasisteady induced load is

$$C_{NQS}=(\partial C_N/\partial z)z(t-\Delta t) \tag{3}$$

where

$$\Delta t=L/\bar{U}=c(\xi_T-\xi_s)/\bar{U}$$

Note that $\bar{U}/U=(C_{Aos}/C_{A0})^{1/2}$ also verified experimentally.[7,8]

The result is an out-of-phase, or rate-dependent, aerodynamic force that can cause aerodynamic undamping for a statically stabilizing force, if a node of the bending mode occurs between the wake source (spike tip) and the submerged body (nose fairing). All this has been well documented in the literature.[2,3,8] Thus, it is redundant to repeat the derivation here, although a brief summary is necessary.

The equation of motion of an elastic vehicle describing single-degree-of-freedom bending oscillations can be written[3]

$$\ddot{q}(t)+2\omega\left[\zeta-\frac{B}{2\omega U}(D_s+D_a)\right]\dot{q}(t)+\omega^2\left[1-\frac{B}{\omega^2}(K_s+K_a)\right]q(t)=f(t) \tag{4}$$

where $B=\rho U^2S/2\hat{m}$ and $f(t)=F(t)/\hat{m}$ is the buffeting force due to random pressure fluctuations.

D_s and D_a are the aerodynamic damping derivatives for separated and attached flow regions, respectively, and negative values denote damping. Multiplication by $-B/2\omega U=-\rho US/4\omega\hat{m}$ puts the aerodynamic damping into the same form as the structural damping ζ, i.e., as a fraction of critical.

One requirement for stability is that the amplitude $q(t)$ be bounded. Thus coefficient of $\dot{q}(t)$ cannot be negative, i.e.,

$$\zeta-(\rho US/4\omega\hat{m})\ (D_s+D_a)\geq 0 \tag{5}$$

This does not preclude limit-cycle oscillations where $\dot{q}(t)$ coefficient $=0$ for $q(t)>0$. Limit cycling can result in structural failure for large limit-cycle amplitude or in fatigue from the continued flexing. A more severe and perhaps a more practical limitation is to specify some minimum acceptable damping to ensure structural integrity, i.e.,

$$\zeta-(\rho US/4\omega\hat{m})\ (D_s+D_a)\geq\zeta_{\min} \tag{6}$$

The aerodynamic damping for infinitesimal amplitude oscillation of the entire missile including the effects of the aerospike is

$$\zeta_a=\frac{-\rho US}{4\omega m}D=-\left[\frac{\rho US}{4\omega m}\right]\ [D_a+D_s] \tag{7}$$

where the damping derivative is

$$D=-C_{N\alpha s}[\phi(\xi_s)]^2-\frac{\Delta^i C_{N\beta}\phi(\xi_s)\phi(\xi_T)}{\bar{\omega}(\xi_T-\xi_s)}\sin\omega\Delta t-2[\phi(\xi_{TE})]^2 \tag{8}$$

The expression is the same as that in Ref. 3, with the exception that the small angle approximations are not used since $\omega\Delta t$ can be as large as 56° at $M=1.0$ for the 58.6 Hz bending mode.

The aerodynamic damping for this critical 58.6 Hz mode is presented in Fig. 3. The modal deflections at the spike tip, $\phi(\xi_T)$, and at the nose fairing $\phi(\xi_s)$, are of opposite sign since a node occurs between ξ_T and ξ_s. Thus, the time-lag term in Eq. (8) is positive or undamping. The result is a negative aerodynamic damping of as much as 1% of critical, illustrating that undamping can result if a node is located between the spike tip and the nose fairing.

Fortunately, the Trident I typically has a structural damping of 3% of critical for this and other modes with a critical first-node location. These damping results are for intinitesimal amplitude oscillations so the mode will decay to $q(t)=0$ ensuring aeroelastic stability.

The aerodynamic loads on the spike itself take longer to respond to a change in attitude since they involve the further time lag associated with upstream convection from reattachment through the recirculation region to the load location on the spike. The situation is similar to the problem of

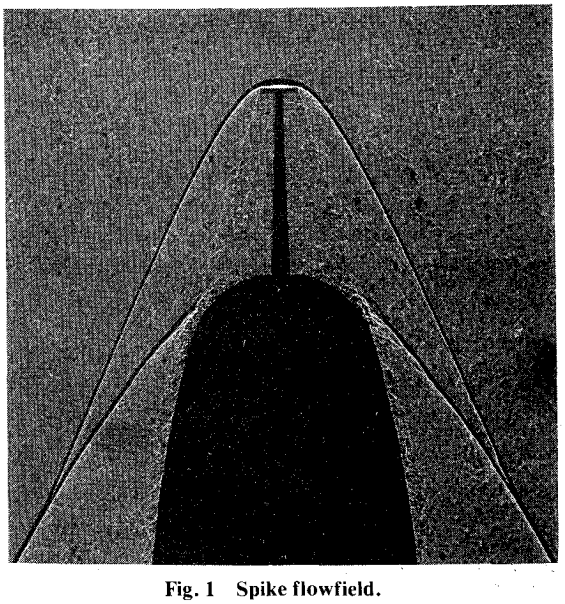

Fig. 1 Spike flowfield.

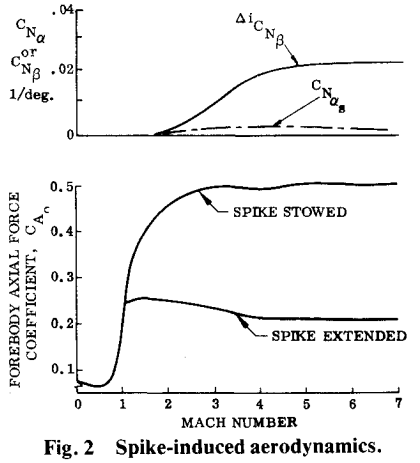

Fig. 2 Spike-induced aerodynamics.

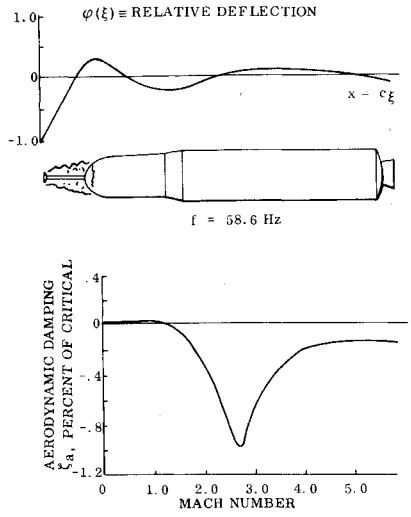

Fig. 3 Aerodynamic damping of critical free-free mode.

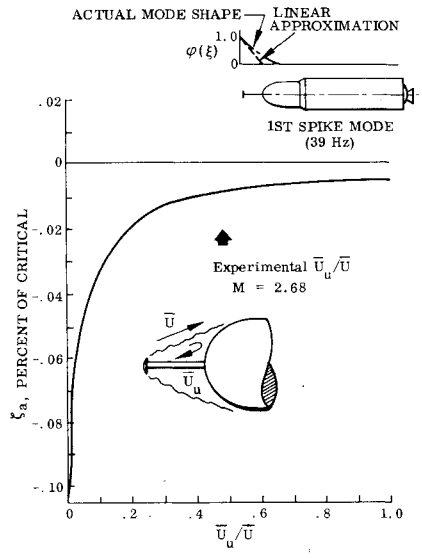

Fig. 4 Aerospike modal damping.

dynamic sting interference.[9] The expression for the spike damping derivative is

$$D=-\frac{\Delta^i C_{m\ddot{\beta}s}\phi(\xi_T)\ \phi'(\xi_s)}{\bar{\omega}(\xi_T-\xi_s)}\sin\ (\omega\Delta t+\omega\Delta t_u^*) \qquad (9)$$

where $\Delta t_u = c(\xi_s-\xi_T)/\bar{U}_u$ is the upstream time lag due to the convection velocity $\bar{U}_u$. Note that in Eq. 9 all the loads on the spike are proportional to spike tip deflection.

The damping is extremely sensitive to upstream communication velocity (Fig. 4). Since $\bar{U}_u$ was not known when the spike design was initiated, it was specified that the spike structural damping had to be 2% of critical to ensure aeroelastic stability. Subsequently, $\bar{U}_u$ was determined from the coherence of fluctuating-pressure wind-tunnel data. This indicates the aerodynamic undamping of the spike will be only 0.01% of critical. Thus, the spike mode is also damped for infinitesimal amplitude oscillations.

Effects of Joint Gaps

During ascent, aerodynamic heating causes the spike joints to expand and eventually they gap and "slop" (a discontinuous load vs deflection curve) occurs. Actually the joint configuration is quite efficient in delaying slop. The forward land and forward tube of each joint (Fig. 5) are exposed to the

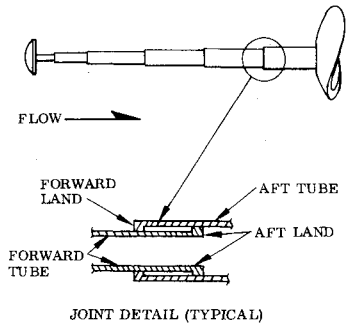

Fig. 5 Spike joint detail.

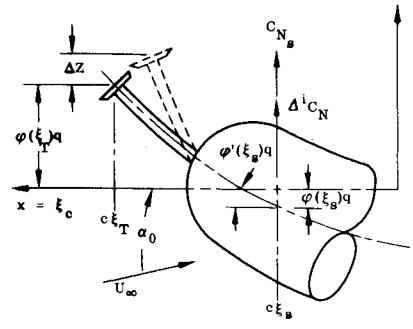

Fig. 6 Coordinate system.

same heating environment, thus they tend to expand at the same rate and remain in contact until well after maximum dynamic pressure occurs. Dynamic analysis and tests of the spike indicate that as long as one land of each joint remains in contact the spike response will be a linear function of the driving force, providing the driving frequency is well above the spike natural frequency. This is exactly the case for modes with a critical first-node location. Thus, slop will not be of practical concern until both lands gap (at $M \approx 5.0$).

Missile Modes

Discontinuous aerodynamic loads have been shown to have a dramatic undamping effect when a flowfield time lag is involved. Significant limit-cycle amplitudes can result with all the attendant dangers. The discontinuous spike deflections suggest a discontinuous (or at least nonlinear) spike-induced load. Thus, it is important to get an assessment of the effects of spike slop.

Figure 6 defines the coordinate system used in the analysis. The spike deflection history is in Fig. 7. For harmonic oscillations the spike deflection without slop is

$$\beta(t)=\alpha_0-\frac{\phi(\xi_s)}{c(\xi_T-\xi_s)}q(t)+\frac{\phi(\xi_T)}{c(\xi_T-\xi_s)}q(t-\Delta t) \qquad (10)$$

where

$$q(t)=\Delta q\ \sin\omega t=\Delta q\, Im[e^{i\omega t}] \qquad (11a)$$

then

$$q(t-\Delta t)=\Delta q\ Im\ [e^{i\omega(t-\Delta t)}]$$
$$=\Delta q\ \sin\omega t\ \cos\omega\Delta t-\Delta q\ \cos\omega t\ \sin\omega\Delta t \qquad (11b)$$

therefore

$$\beta(t)=\alpha_0+\frac{\phi(\xi_T)}{c(\xi_T-\xi_s)}\Delta q(\sin\psi\cos\gamma-\cos\psi\ \sin\gamma)$$
$$-\frac{\phi(\xi_s)}{c(\xi_T-\xi_s)}\Delta q\ \sin\psi \qquad (12)$$

where $\psi=\omega t$ and $\gamma=\omega\Delta t$.

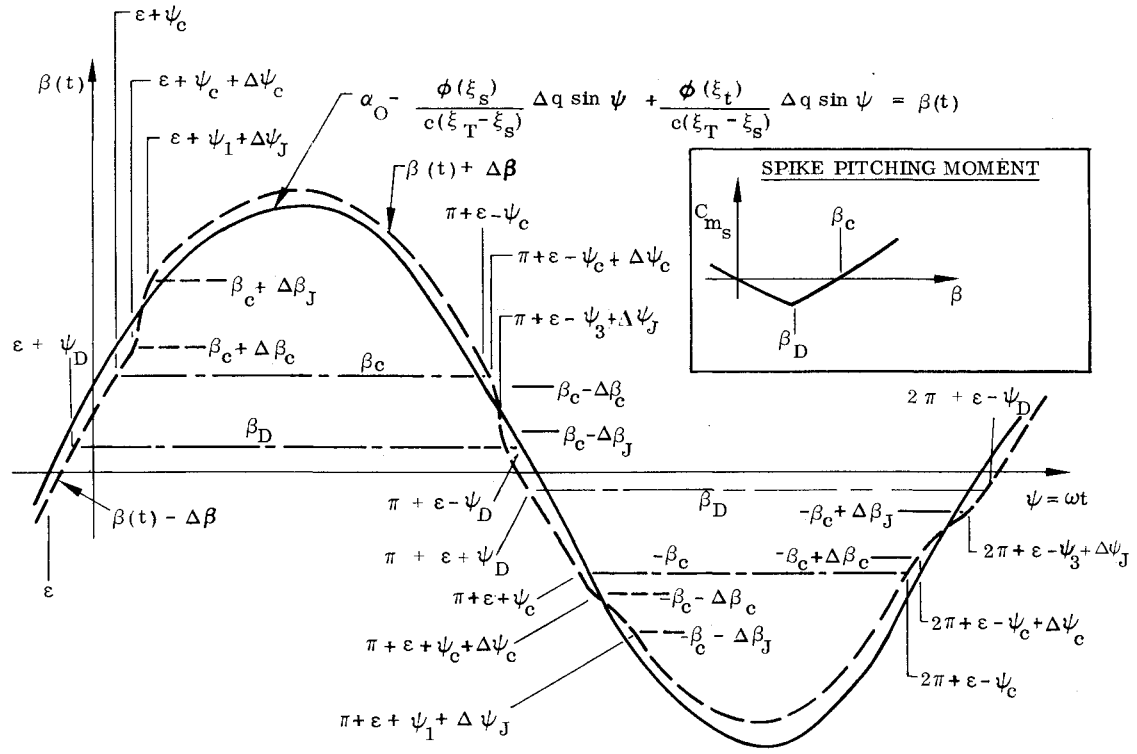

Fig. 7 Spike deflection history.

Defining

$$\tan\epsilon = \phi(\xi_T)\sin\gamma / [\phi(\xi_T)\cos\gamma - \phi(\xi_s)]$$

one can write

$$\beta(t) = \alpha_0 + \left[\frac{\phi(\xi_T)\cos\gamma - \phi(\xi_s)}{c(\xi_T-\xi_s)\cos\epsilon}\right]\Delta q \sin(\psi-\epsilon) \qquad (13)$$

The deflection history with slop is sensitive to the spike pitching moment coefficient, C_{ms}, sketched in the insert of Fig. 7. When the maximum oscillation amplitude is less than the slop, i.e., $\beta(t) \le \Delta\beta$ (where $\Delta\beta = (\Delta z/c)\ (\xi_T - \xi_s)$ is the slop) the stable $C_{m\beta s}$ will cause the spike to remain at $\beta = 0$ and $\Delta' C_{m\beta} = 0$. When $\beta(t) > \Delta\beta$ the spike tip will respond to the missile-bending modes. The slop at $\beta = 0$ will no longer affect the spike displacement since the aerodynamic frequency of the spike is at least two orders of magnitude less than the critical modal frequency.

At $\beta(t) = \beta_c$ the spike moment again passes through zero, but this time $C_{m\beta s}$ is destabilizing. This occurs where

$$\psi_c = \sin^{-1}\left\{\frac{(\beta_D - \alpha_0)c(\xi_T-\xi_s)\cos\epsilon}{[\phi(\xi_T)\cos\gamma - \phi(\xi_s)]\Delta q}\right\} \qquad (14)$$

The unstable $C_{m\beta s}$ will tend to drive the spike through the slop from $\beta(t) - \Delta\beta$ to $\beta(t) + \Delta\beta$. However, the spike will not begin to move immediately when $\psi = \epsilon + \psi_c$ since the spike load lags the spike tip position due to the convection time lag downstream to reattachment and upstream through the recirculation region. This additional time lag is $\Delta\psi_c = 3\omega c(\xi_T - \xi_s)/\bar{U}$.

Accounting for the acceleration of the spike through the slop by the unstable spike load gives the following expression for the jump lag

$$\Delta\psi_J = \left\{\frac{2\Delta z}{c(\xi_T-\xi_s)}\left\{\frac{\Delta\ddot{\beta}}{2\omega^2} + \left[\frac{\phi(\xi_T)-(\xi_s)}{c(\xi_T-\xi_s)}\right]\Delta q \sin(\psi_c + \Delta\psi_c)\right\}^{-1}\right\}^{1/2} \qquad (15)$$

where

$$\omega\Delta t_J = \Delta\psi_J$$

The discontinuities in the $\beta(t)$ curve in Fig. 7 may be defined from Eq. 14 and 15 as follows

$$\psi_1 = \psi_c + \Delta\psi_c \qquad \psi_3 = \psi_c - \Delta\psi_c$$
$$\psi_2 = \psi_1 + \Delta\psi_J \qquad \psi_4 = \psi_3 - \Delta\psi_J \qquad (16)$$

Aerodynamic Damping with Slop

The highly nonlinear $\beta(t)$ curve requires special techniques. The technique of Ref. 11 is followed where the effective damping derivative ($\bar{D}$) is computed from the energy dissipation (E) during one cycle of oscillation (period T).

$$\bar{D} = \frac{\phi(\xi_s)_c}{\pi\omega\Delta q c/U}\int_{\psi_0}^{\psi_0+2\pi} C_N(\psi)\cos\psi d\psi \qquad (17)$$

where $2\pi = \omega T$, and $\psi_0 = \epsilon$ (Fig. 7). Likewise an effective aerodynamic spring can be defined

$$\bar{K}_\alpha = \frac{\rho U^2 S}{\Delta q^2} c^2 \phi'(\xi_s)\int_0^{\Delta q} Cm(q)\, q dq \qquad (18)$$

For $\beta(t) \le \Delta\beta$

$$C_N(\psi) = C_{N0}(\psi) = C_{N\alpha s}\left[\alpha_0 + \frac{\phi(\xi_s)}{c(\xi_T-\xi_s)}\Delta q \sin\psi - \frac{\phi(\xi_s)}{c(\xi_T-\xi_s)}\Delta q \frac{\omega}{U}\cos\psi\right] \qquad (19)$$

substituting Eq. 19 into Eq. 17 and integrating gives

$$\bar{D}_s = -C_{N\alpha s}[\psi(\xi_s)]^2 \qquad (20)$$

For $\beta(t) > \Delta\beta$, $C_n(\psi)$ varies throughout the cycle, thus

$$C_{N1}(\psi) = C_{N0}(\psi) + \Delta^i C_{N\beta}\left\{\alpha_0 - \frac{(\xi_s)}{c(\xi_T - \xi_s)}\Delta q \sin\psi + \frac{\phi(\xi_T)}{c(\xi_T - \xi_s)}\Delta q[\sin\omega t \cos\omega\Delta t - \cos\omega t \sin\omega\Delta t] - \frac{\Delta z}{c(\xi_T - \xi_s)}\right\}$$

for $\epsilon \to \epsilon + \psi_1$ and $\pi + \epsilon - \psi_4 \to \pi + \epsilon + \psi_4$

$$C_{N2}(\psi) = C_{N1}(\psi) + \Delta^i C_{N\beta}\left[\frac{2\Delta z}{c(\xi_T - \xi_s)}\right]$$

for $\epsilon + \psi_2 \to \pi + \epsilon - \psi_3$ and $\pi + \epsilon + \psi_2 \to 2\pi + \epsilon - \psi_3$,

$$C_{NJ1}(\psi) = C_{N1}(\psi) + \Delta^i C_{N\beta}\left[\frac{2\Delta z}{c(\xi_T - \xi_s)(\Delta\psi_J - \Delta\psi_c)}\right]$$

for $\epsilon + \psi_1 \to \epsilon + \psi_2$ and $\pi + \epsilon + \psi_1 \to \pi + \epsilon + \psi_2$,

$$C_{NJ2}(\psi) = C_{N2} - \Delta^i C_{N\beta}\left[\frac{2z}{c(\xi_T - \xi_s)(\Delta\psi_J - \Delta\psi_c)}\right]$$

for $\pi + \epsilon - \psi_3 \to \pi + \epsilon - \psi_1$.

Substituting for $C_N(\psi)$ and integrating gives

$$\bar{D}_s = -C_{N\alpha s}[\phi(\xi_s)]^2 - \frac{\Delta i C_{N\beta}}{\bar{\omega}(\xi_T - \xi_s)}\left\{\phi(\xi_s)\phi(\xi_T)\sin\omega\Delta t - \frac{2\Delta z\,\phi(\xi_s)}{\Delta q}\left\{\left[\frac{\sin(\epsilon+\psi_1) - \sin(\epsilon+\psi_2)}{(\Delta\psi_J - \Delta\psi_c)}\right] + \left[\frac{\sin(\epsilon-\psi_3) - \sin(\epsilon-\psi_4)}{(\Delta\psi_J - \Delta\psi_c)}\right]\right\}\right\} \quad (21)$$

for $\beta(t) > \Delta\beta$.

The attached flow damping is calculated from first-order momentum theory,[12]

$$D_a = -2[\phi(\xi_{TE})]^2 \quad (22)$$

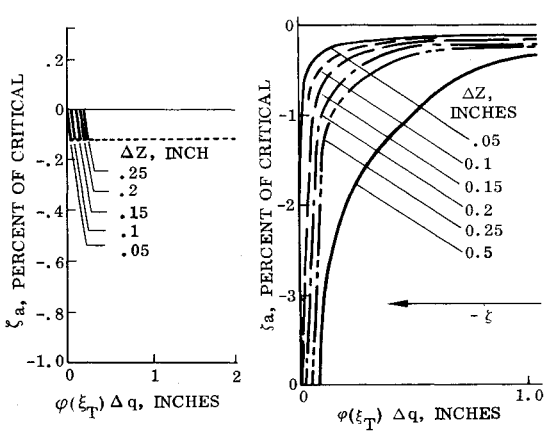

a) $\alpha_0 = 0$; M = 5.0 b) $\alpha_U = 3.75°$, M = 5.0

Fig. 8 Aerodynamic damping for critical missile mode (58.6 Hz) with spike slop. a) $\alpha_0 = 0$. $M = 5.0$. b) $\alpha_U = 375°$, $M = 5.0$.

Spike Mode

Not only is the damping derivative of the spike mode dominated by slop, but the spring constant is too. When the spike traverses the slop region the structural spring, K (Eq. 4) is zero (i.e., $\omega^2 = \bar{K} = 0$). The aerodynamic spring is given in Eq. 18.

Likewise for the structure

$$\bar{K} = \frac{2}{\Delta q^2}\int_0^{\Delta q} K(q)\, q\,dq \quad (23)$$

and

$$\omega = [(\bar{K}/\hat{m}) - B(K_s + K_a)]^{1/2}$$

Integrating Eq. 18 from $-\Delta q$ to Δq gives

$$\omega^2 = \frac{\bar{K}}{\hat{m}}\left[1 - \frac{\Delta z^2}{\Delta q^2}\right] - \frac{\rho U^2 Sc}{2\hat{m}}\phi'(\xi_s)\left\{\Delta^i Cm_{\beta I}\left[\frac{\phi(\xi_T)}{c(\xi_T - \xi_s)}\frac{z_D{}^2}{\Delta q^2}\right] + \Delta^i Cm\beta_2\left[\frac{\phi(\xi_T)}{c(\xi_T - \xi_s)}\left(1 - \frac{z_D{}^2}{\Delta q^2}\right) + \frac{2\alpha_0}{\Delta q^2}(\Delta q - z_D)\right]\right\} \quad (24)$$

for $\beta < \beta_D$, $\Delta^i Cm\beta_2 = 0$, $z_D = \Delta q$ and *for* $\beta \le \Delta\beta$, $\Delta z = \Delta q$, as well as for $\beta(t) > \beta_D$, $\Delta^i Cm\beta_1 = 0$, $z_D = \Delta q$, where $\beta_D = (z_D/c)(\xi_T - \xi_s)$.

The expression for the spike damping is derived by integrating Cm over the cycle where the entire spike load is considered to be induced and is a function of the recirculatory time lag

$$\Delta t = c(\xi_T - \xi_s)\left(\frac{1}{\bar{U}} + \frac{1}{\bar{U}_u}\right) \quad (25)$$

The spike damping is

$$\bar{D} = \frac{\phi'(\xi_s)c^2}{\pi\bar{\omega}\Delta q}\int_{\epsilon}^{\epsilon+\psi_D} Cm(\psi)\cos\psi\, d\psi \quad (26)$$

where $Cm(\psi)$ varies throughout the cycles as follows;

$$C_m(\psi) = \Delta^i Cm_{\beta A}\beta(t - \Delta t)$$

for $\epsilon \to \epsilon + \psi_D$, $\pi + \epsilon + \psi_D \to \pi + \epsilon + \psi_D$, $2\pi + \epsilon - \psi_D \to 2\pi + \epsilon$

$$C_m(\psi) = \Delta^i Cm_{\beta B}\beta(t - \Delta t)$$

for $\epsilon + \psi_D \to \pi + \epsilon + \psi_D$, $\pi + \epsilon - \psi_D \to 2\pi + \epsilon - \psi_D$

and

$$\beta(t - \Delta t) = \alpha_0\left[\frac{\phi(\xi_T)}{c(\xi_T - \xi_s)}\right]\Delta q \sin(\psi - \epsilon)$$

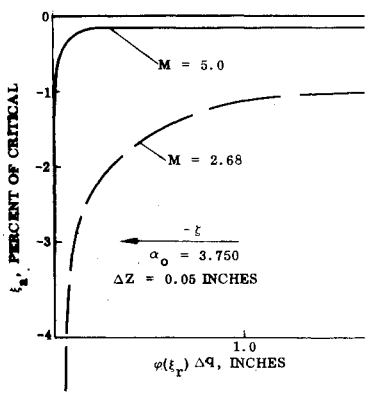

Fig. 9 Effect of stop delay on aerodynamic damping.

also

$$\psi_D = \sin^{-1}\left[\frac{(\beta_D-\alpha_0)c(\xi_T-\xi_s)}{\phi(\xi_T)\Delta q}\right]$$

integrating gives

$$D=\frac{c^2}{\pi\bar{\omega}}\frac{\phi'(\xi_s)\,\phi(\xi_T)}{c(\xi_T-\xi_s)}\left\{\Delta^i Cm_{\beta A}\left\{\frac{\cos\epsilon\,\sin 2\epsilon\,\sin 2\psi_D}{2}\right.\right.$$

$$-\sin\epsilon\left[\sin 2(\epsilon+\psi_D)-\sin 2(\epsilon-\psi_D)\right]\Big\}+\Delta^i Cm_{\beta B}$$

$$\left[\frac{\cos\epsilon\,\sin 2\epsilon\,\sin 2\psi_D}{2}\right]-\sin\epsilon[\pi+\sin 2(\epsilon-\psi_D)$$

$$\left.-\sin 2(\epsilon+\psi_D)]\right\} \qquad (27)$$

where, if $\alpha_0 \le \beta_D$, then $\Delta^i Cm_{\beta A}=\Delta^i Cm\beta_1$, $\Delta^i Cm_{\beta B}=\Delta^i Cm_{\beta 2}$, and if $\beta(t)\le\beta_D$, then $\psi_D=0$, $\Delta^i Cm_{\beta A}=\Delta^i Cm_{\beta B}=\Delta^i Cm_{\beta 1}$. Furthermore if $\alpha_0>\beta_D$

$$\Delta^i Cm_{\beta A}=\Delta^i Cm\beta_2 \qquad \Delta^i Cm_{\beta B}=\Delta^i Cm_{\beta 1}$$

also if $\beta(t)>\beta_D$, then $\psi_D=0$, $\Delta^i C_{\beta A}=\Delta^i Cm_{\beta B}=\Delta^i Cm_{\beta_2}$

Discussion of Results

As expected, the spike slop adds to the undamping. Figure 8 shows the damping of the critical 58.6 Hz missile mode plotted against the displacement of the spike tip $\phi(\xi_T)\,\Delta q$ for two trim angles of attack $\alpha_0=0°$ and 3.75°. The latter is the critical case since the $\beta(t)$ nonlinearity occurs as the spike passes through the null position maximizing its effect on the out-of-phase moment. Effectively a hysteresis results in $\Delta^i C_N$ due to the overshoot of β_c by the amount of $\Delta\beta_c \sim \Delta\psi_c$. The hysteresis loop constitutes an energy input into the vehicle that is undamping. When the hystereses is small relative to the rest of the cycle the damping approaches the no slop value (i.e., for large $\phi(\xi_T)\Delta q$). Fortunately the limit cycle amplitude at $\zeta_a=-\zeta$ is negligible and the structure is not overstressed.

For $\alpha_0=0$ the mode is initially damped as the spike remains centered at $\beta(t)=0$. As Δq is increased, the damping approaches the no slop value. The effect of the discontinuity at $\beta(t)=\beta_c$ is negligible.

Had slop occurred at $M=2.68$ where the aerodynamic effects are a maximum a significant limit cycle oscillation would have resulted that could have endangered the structure (Fig. 9). Thus, the delay of slop due to a double land spike joint design significantly reduces the limit-cycle oscillations.

Figure 10 presents similar results for the spike (39 Hz) mode. Also included in the figure is the effect of slop on spike frequency. For the spike mode $\alpha_0=0$ is the critical case. Limit cycle oscillations do not occur since the 2% of critical structural damping overpowers the −0.38% aerodynamic undamping. Aerodynamic effects on the spike are negligible since the spike is submerged in low-energy separated flow.

Fluctuating Pressures

Up to now, the discussion has been concerned only with the left-hand side of Eq. (4). The right-hand side, the forcing function due to random pressure fluctuations, was obtained experimentally from a wind-tunnel test.[10]

The overall transonic fluctuating pressure distribution along the spike at $\alpha>0$ gave the most surprising result. Peak-pressure fluctuations occurred on the lateral meridians of the spike rather than on the windward side, as expected (Fig. 11). Flow visualization results suggest the flow model sketched in Fig. 12. The separation region is neither axisymmetric, not closed at $\alpha>0$ as it is at $\alpha=0$. Instead it resembles a horseshoe vortex with the separated region being vented via a pair of

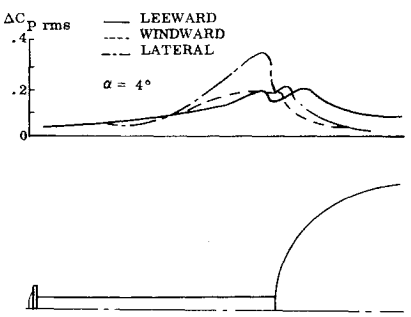

Fig. 11 Fluctuating pressure distributions.

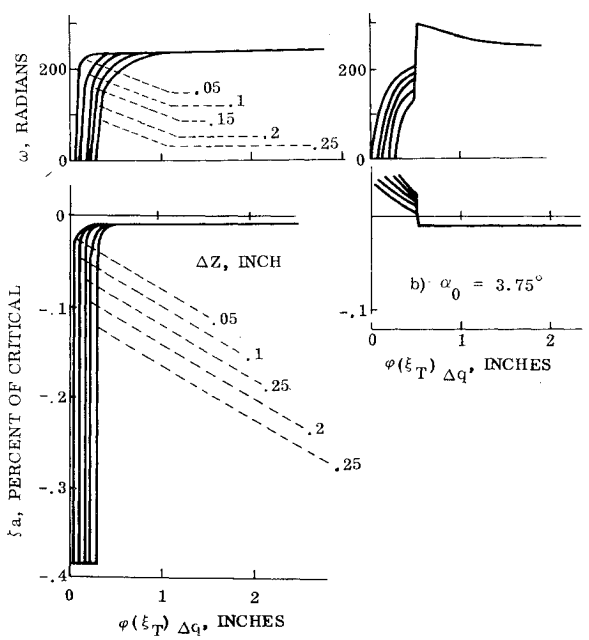

Fig. 10 Effect of slop on spike frequency and damping.

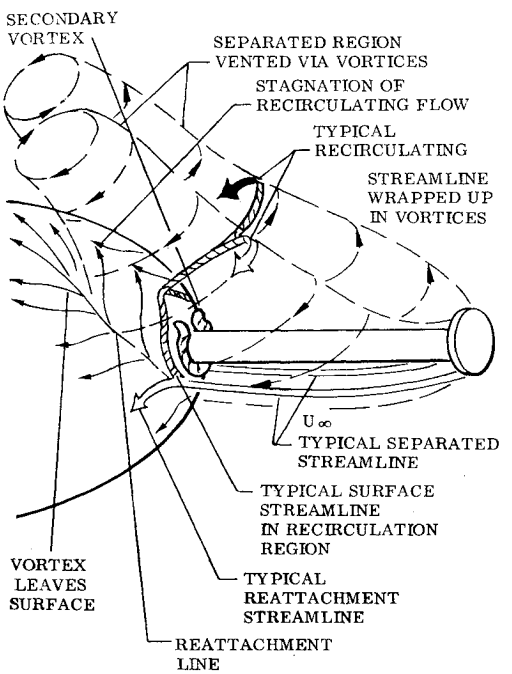

Fig. 12 Spike-induced flowfield ($\alpha>0$).

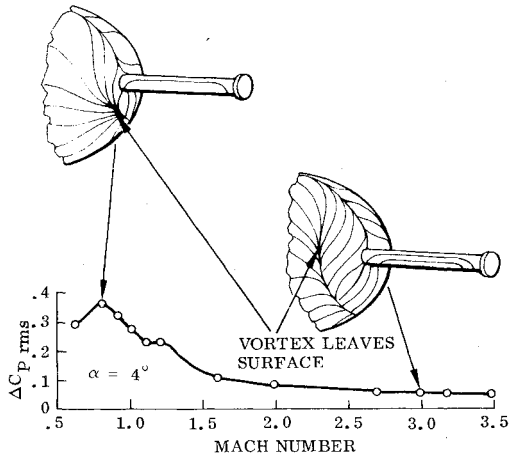

Fig. 13 Correlation of vortex separation point with fluctuating pressures on the side of the spike base.

vortices that are shed downstream over the shoulder. The points where these vortices leave the surface are indicated by the source-like oil streaks that terminate the feathery reattachment line. These points seem to be the key to the elevated pressure fluctuations on the spike sides. At transonic speeds, the streak lines emanating from the vortex detachment points impinge on the spike sides, whereas, they miss the spike altogether at supersonic speed (Fig. 13). It is believed that the flow impinging from the vortex detachment point somehow interacts with the shedding of the secondary vortices causing the high-pressure fluctuations on the spike sides.

The power spectral-density measurements, scaled to flight conditions, constituted the input to the "RPI Random Response Program," which was used to determine the spectral-density response to the random pressure field.[13] Results for the first spike mode (39 Hz mode) predicted a root-mean-square bending moment at the spike base of 3060 in. lb, compared to an allowable of 3800 in. lb rms. This fluctuating pressure load is the critical lateral load on the spike. The static aerodynamic load is relatively insignificant (21 in. lb maximum) because the spike is submerged in low-energy separated flow.

Conclusions

The drag reduction spike has an adverse effect on the aerodynamic damping of critical missile and spike modes as was recognized from the outset of the design. Slop increases the aerodynamic undamping resulting in limit cycle oscillations. However, because of the double land design of the Trident I aerospike, slop was delayed until well after maximum dynamic pressure. Thus, the aerodynamic undamping was small resulting in a negligible limit cycle amplitude. Furthermore, the large pressure fluctuations in the spike-induced separated-flow region are responsible for virtually the entire root-bending moment on the spike.

Structural integrity of the Trident I is assured due to the large structural damping that overcomes the spike-induced aerodynamic undamping, and keeps limit-cycle oscillations to an acceptable level. However, this may not be the case for another vehicle. Thus, when considering a flow separation spike for drag reduction, a detailed aeroelastic analysis should be conducted to insure structural integrity of the vehicle and aerospike.

References

[1]French, N.J. and Jecmen, D.M., "Transonic/Supersonic Wind Tunnel Investigation of Effects of Parametric Variations in Nose Fairing and Aerospike Geometry on Trident I C4 Missile Body Static Stability and Drag," Lockheed Missiles and Space Co., Sunnyvale, Calif., LMSC-D366908, Sept. 1974.

[2]Ericsson, L.E. and Reding, J.P., "Dynamics of Separated Flow Over Blunt Bodies," LMSC-2-80-65-1, Dec. 1965.

[3]Ericsson, L.E. and Reding, J.P., "Analysis of Flow Separation Effects on the Dynamics of a Large Space Booster," *Journal of Spacecraft and Rockets*, Vol. 2, July-Aug. 1962, pp. 481-490.

[4]French, N.J., "Investigation of Static Stability and Axial Force of Trident I C4 Configurations in the AEDC Tunnel B, Volume I First Stage, Second Stage, and Nose Fairing Alone With and Without Aerospike," LMSC-L015007, Jan. 1972.

[5]Reding, J.P., "Forces Induced on Bodies in Free Wakes and Three-Dimensional Cavities," LMSC-667990, Dec. 1962.

[6]Jecmen, D.J., Reding, J.P., and Ericsson, L.E., "An Application of Automatic Carpet Plotting to Wind-Tunnel Data Reductions," *Journal of Spacecraft and Rockets*, Vol. 4, March 1967, pp. 408-410.

[7]Reding, J.P., "Partial Simulation of Elastic Body Dynamics for the Upper-Stage Apollo-Saturn Launch Vehicle," LMSC M-36-67-4, Dec. 1967.

[8]Ericsson, L.E., Reding, J.P., and Guenther, R.A., "Analytic Difficulties in Predicting the Effects of Separated Flow," *Journal of Spacecraft and Rockets*, Vol. 8, Aug. 1971, pp. 872-878.

[9]Reding, J.P. and Ericsson, L.E., "Dynamic Support Interference," *Journal of Spacecraft and Rockets*, Vol. 9, July 1972, pp. 547-553.

[10]Guenther, R.A., "Analyses of Fluctuating Pressure Tests of the C4A Candidate Nose Fairing," LMSC-D366982, April 1975.

[11]Ericsson, L.E., "Aeroelastic Instability Caused by Slender Payloads," *Journal of Spacecraft and Rockets*, Vol. 4, June 1967, pp. 65-73.

[12]Bisplinghoff, R.L., Ashley, H., and Halfman, R.L., *Aeroelasticity*, Addison-Wesley, Cambridge, Mass., 1955.

[13]Hertzberg, R.J., "RPI Random Response Program," LMSC TM 54/56-33, 1965.